




Magnesium Green for fluorometric measurement of ATP production does not interfere with mitochondrial respiration

 Luiza HD Cardoso*,  Carolina Doerrier,  Erich Gnaiger

Oroboros Instruments, Innsbruck, Austria

*Corresponding author: luiza.cardoso@orooboros.at

Posted Online 2021-01-29

Abstract

For the advanced study of mitochondrial function, high-resolution respirometry is extended by fluorometric measurement of ATP production using the fluorophore Magnesium Green™ (MgG). A common problem with several fluorescent dyes is the inhibition of mitochondrial respiration. In the present study, a coupling control protocol was applied in combination with MgG to measure ATP production simultaneously with respiration for calculation of P_{O_2}/O_2 ratios. MgG at 1.1 μM did not affect respiration through the NADH-linked and succinate-linked pathways. Respiration was not inhibited in any of the coupling control states, hence coupling control efficiencies were not affected by MgG.

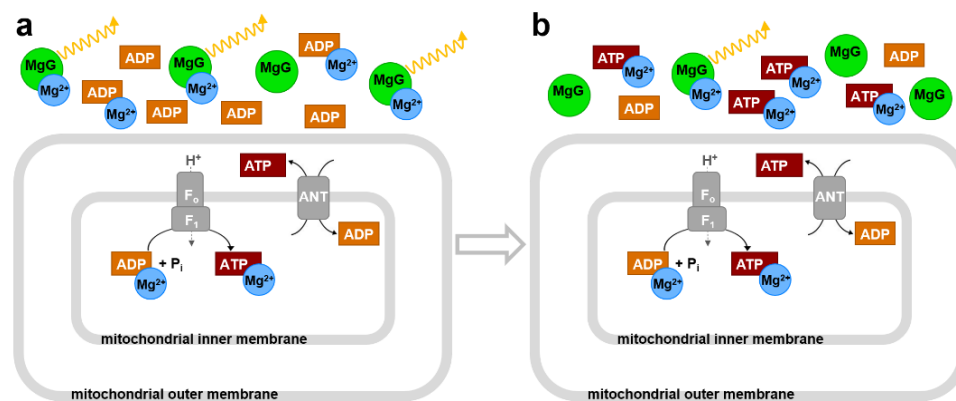
Keywords – ATP; ATP production; high-resolution respirometry; Magnesium Green; mitochondria; oxidative phosphorylation; fluorometry; FluoRespirometry

1. Introduction

Mitochondrial ATP production can be analyzed with a fluorometric technique using Magnesium Green™ (MgG) as a fluorescent probe, as described by Chinopoulos et al (2009). Application of the Mg^{2+} -sensitive fluorophore as an indicator of ATP production relies on the fact that ADP and ATP have different affinities for Mg^{2+} (Gnaiger, Wyss 1994; Leyssens et al 1996; Budinger et al 1998). ADP is phosphorylated to ATP in the mitochondrial matrix. In the phosphorylation system ADP/ATP and inorganic phosphate P_i are exchanged stoichiometrically by the adenine nucleotide translocase ANT and the phosphate carrier PiC. Under experimental conditions when ADP decreases while ATP increases in the extramitochondrial milieu, the Mg^{2+} concentration declines due to the higher affinity for Mg^{2+} of ATP than ADP (Figure 1). Therefore, the fluorometric assay with the membrane-impermeant MgG provides a quantitative approach to analyze mitochondrial ATP production. This method was developed further to measure concomitantly mitochondrial ATP production and O_2 consumption in the Oroboros O2k-

35 Fluorescence Respirometer which is an experimental system complete for high-resolution
36 respirometry including fluorometry (Chinopoulos et al 2014).

37 Fluorescent dyes are widely used to assess various parameters relevant in
38 mitochondrial physiology. Safranin, rhodamine and its derivatives, such as TMRM, are
39 frequently employed as reporters of the mitochondrial membrane potential $\Delta\Psi_{p+}$.
40 However, all $\Delta\Psi_{p+}$ dyes have been shown to affect mitochondrial respiration (Scaduto,
41 Grotjohann 1999). Like TPP⁺, safranin mainly affects the NADH (N)-linked pathway, the
42 phosphorylation system, and to a smaller extent the succinate (S)-linked pathway
43 (Krumnschnabel et al 2014). The effect of $\Delta\Psi_{p+}$ fluorescent probes can be explained since
44 they accumulate in the mitochondrial matrix and thus possibly affect mitochondrial
45 function.



46 **Figure 1. Concept of the MgG assay according to Chinopoulos et al (2014).** MgG
47 fluoresces when bound to Mg²⁺. ADP and ATP compete for Mg²⁺ binding with different
48 affinities; ATP has a higher affinity for Mg²⁺ compared to ADP. **(a)** Initial experimental
49 conditions, when ADP is added, binding some Mg²⁺, and high MgG fluorescence drops
50 slightly. **(b)** As the experiment proceeds, ADP is phosphorylated to ATP, which is
51 exchanged for ADP by the adenine nucleotide translocase ANT. With increase in ATP in
52 the extramitochondrial medium, more Mg²⁺ is bound to ATP, and MgG fluorescence
53 decreases.

54 It is important to note that another dye frequently used in mitochondrial physiology
55 studies, Amplex UltraRed, employed to analyze H₂O₂ production, was shown to affect
56 mitochondrial respiration even though the mitochondrial membranes are not permeable
57 to this fluorophore (Makrecka-Kuka et al 2015). Therefore, it is important to analyze
58 whether MgG affects mitochondrial respiration, despite the fact that mitochondrial
59 membranes are not permeable to this fluorophore.

60 In the present technical communication, we report the effect of MgG on
61 mitochondrial respiration, which is the gold standard to evaluate mitochondrial function.
62 This provides an important contribution towards further development of this method to
63 analyze P_o/O₂ ratios in different mitochondrial preparations. The use of a coupling
64 control protocol assessing O₂ consumption and MgG fluorescence allows for the
65 evaluation of mitochondrial respiration and ATP production using NADH- and succinate-
66 linked substrates in LEAK, OXPHOS- and ET-state, making it possible to obtain flux control
67 efficiencies.

68 2. Materials and methods

69 2.1. Reagents

70 Magnesium Green was purchased from Invitrogen/Thermo Fisher Scientific (cat. N°
71 M3733). Antimycin A (cat. N° A8674), ATP (cat. N° A2383), CCCP (cat. N° C2759), malate
72 (cat. N° M1000), MgCl₂ 1 M (cat. N° M1028), oligomycin (cat. N° O4876), pyruvate (cat.
73 N° P2256), rotenone (cat. N° R8875), SF 6847 (cat. N° T182), and succinate (cat. N°
74 S2378) were obtained from Sigma Aldrich. ADP was acquired from Millipore (cat. N°
75 117105), and carboxyatractyloside from Calbiochem (cat. N° 216201).

76 ADP and ATP were diluted in deionized H₂O without addition of Mg²⁺ salts, pH was
77 adjusted to 6.9 with KOH. Magnesium Green, malate, succinate, carboxyatractyloside and
78 MgCl₂ were diluted in deionized H₂O whereas antimycin A, CCCP, oligomycin, rotenone
79 and SF 6847 were diluted in ethanol p.a. All solutions were aliquoted and stored at -20 °C,
80 except pyruvate, which was diluted in deionized H₂O fresh on the day of each experiment.

81 2.2. Animals

82 Wild-type C57BL/6N adult mice (*N*=3 per experimental group) were housed in the
83 animal facility of the Medical University of Innsbruck (maximum 5 mice per cage) and,
84 maintained at 22 °C with a controlled 12 h light/dark cycle. Mice were fed *ad libitum* with
85 free access to water. All procedures were conducted according to the Austrian Animal
86 Experimentation Act in compliance with the European convention for the protection of
87 vertebrate animals used for experimental and other scientific purposes
88 (Tierversuchsgesetz 2012; Directive 2010/63/EU; BMWFM-66.011/0128-
89 WF/V/3b/2016).

90 2.3. Cardiac mitochondrial isolation and protein concentration determination

91 Following cervical dislocation, the hearts were immediately excised and transferred
92 into ice-cold biopsy preservation solution (BIOPS: 10 mM Ca²⁺-EGTA - 0.1 μM free Ca²⁺,
93 20 mM imidazole, 20 mM taurine, 50 mM K⁺-MES, 0.5 mM dithiothreitol, 6.56 mM MgCl₂,
94 5.77 mM ATP, 15 mM phosphocreatine, pH 7.1 adjusted with KOH) for short period of
95 time (1–2 h; Fontana-Ayoub et al 2016). All procedures were performed on ice (Gnaiger
96 et al 2000a). Mouse heart mitochondria were isolated following the protocol described
97 by Fontana-Ayoub and Krumschnabel (2015). The heart (~ 80–120 mg) was washed to
98 remove blood clots and minced with 1 mL of BIOPS. The tissue was homogenized with 2
99 mL isolation buffer (IB1: 0.5 M mannitol; 0.5 M sucrose; 0.1 M EGTA; pH 7.4 adjusted with
100 Tris; 2.5 mg/mL BSA and 0.5 mg/mL subtilisin, the latter two added freshly on the day of
101 use) on a 10 mL glass-Teflon Potter Elvehjem homogenizer, 6–8 × with about 1000 rpm
102 mechanical rotation. 3 mL of IB1 was added to the homogenate which was centrifuged at
103 800 *g* for 10 min at 4 °C. The supernatant was centrifuged again, at 10 000 *g* for 10 min at
104 4 °C. The pellet was resuspended carefully using a 1 mL pipette in 0.5 mL IB2 (IB1 without
105 subtilisin). After addition of 2 mL IB2, the homogenate was centrifuged again at 10 000 *g*
106 for 10 min at 4 °C. The pellet was resuspended in 200 μL of IB3 (IB1 without BSA and
107 subtilisin) and kept on ice until use on the same day within 2 h.

108 Protein concentration was used for calculation of mass specific O₂ flux, determined
 109 using the kit DC Protein Assay (Bio-Rad, Hercules, CA, US). Absorbance was measured at
 110 620 nm with a Tecan Infinite TM F200 spectrophotometer (Tecan, Männedorf,
 111 Switzerland), using BSA at different concentrations as standards (Lowry et al 1951).

112 *2.4. High-resolution respirometry*

113 Oxygen consumption and ATP production measurements were performed
 114 simultaneously at 37 °C in the O2k-FluoRespirometer (O2k, Oroboros Instruments,
 115 Innsbruck, Austria). The O2k includes two Duran® glass chambers with stirring (750
 116 rpm) and controlled temperature for closed-chamber respirometry using polarographic
 117 oxygen sensors (POS). Smart Fluo-Sensors Blue were used, with excitation LED 465 nm
 118 and filters for the LED and photodiode selected for Magnesium Green™). Specific
 119 amperometric emission and detection settings – fluorescence light intensity of 500 and
 120 gain 100 – were applied with the software DatLab 7.4 (Oroboros Instruments, Innsbruck,
 121 Austria) with continuous data recording set at 2 s time intervals. Standardized
 122 calibrations and instrumental O₂ background tests were performed (Doerrier et al 2018).
 123 The time-derivative of the O₂ concentration is calculated real-time by DatLab, providing
 124 traces of O₂ flux corrected for the O₂ instrumental background (Gnaiger 2001).

125 Experiments were run with cardiac isolated mitochondria at protein concentrations
 126 in the range of 0.026–0.049 mg/mL in modified mitochondrial respiration medium
 127 MiR05-MgG (MgCl₂ 1 mM instead of 3 mM in MiR05, EGTA 0,5 mM, KH₂PO₄ 10 mM, Hepes
 128 20 mM, lactobionic acid 60 mM, D-sucrose 110 mM, taurine 20 mM, BSA 1 g/L, pH
 129 adjusted with KOH to 7.1). This modification of MiR05 (Gnaiger et al 2000a) was
 130 optimized for measurement of ATP production with MgG.

131 *2.5. ATP production measurement with MgG*

132 MgG (Magnesium Green™, pentapotassium salt, cell impermeant) does not
 133 permeate biological membranes. Therefore, the plasma membrane barrier function must
 134 be removed, as achieved in mitochondrial preparations – isolated mitochondria, tissue
 135 homogenates, permeabilized tissues and cells. MgG remains outside of the mitochondrial
 136 matrix and fluoresces when bound to Mg²⁺. In the phosphorylation reaction



138 reactants and MgG bind Mg²⁺ according to their apparent dissociation constants. When
 139 ADP is added to the experimental chamber, there is a fast drop of the fluorescence signal.
 140 If mitochondria and fuel substrates are present, ATP is generated and exchanged with
 141 ADP by the ANT. ATP has a higher affinity to Mg²⁺ compared to ADP. As ATP concentration
 142 increases in the medium, the free Mg²⁺ concentration declines, less MgG is bound to Mg²⁺,
 143 and the fluorescence decreases. The ATP concentration in the medium is calculated
 144 according to Chinopoulos et al (2009; 2014), taking in account that: (1) the initial
 145 concentration of ATP is zero, (2) the initial concentration of ADP is known, (3) the
 146 concentration of Mg²⁺ is measured, and (4) apparent K_d values for ADP and ATP with Mg²⁺
 147 are obtained experimentally.

148 The free Mg^{2+} concentration was calibrated in MiR05-MgG containing the
149 mitochondrial sample, fuel substrates, carboxyatractyloside, and oligomycin. $MgCl_2$ was
150 titrated in 10 steps of 0.1 mM to obtain a non-linear fit for calibration of the amperometric
151 signal. After calibration, the K_d of ADP and ATP for Mg^{2+} was determined for each
152 experimental condition by performing multiple titrations with ADP or ATP.

153 2.6. *Substrate-uncoupler-inhibitor-titration (SUIT) protocols*

154 Coupling control protocols (SUIT-006) assess different coupling control states -
155 LEAK, OXPHOS and ET - at a constant electron-transfer-pathway state (Gnaiger et al
156 2020). The effect of MgG on mitochondrial respiration was evaluated in its absence or
157 presence (1.1 μM), which was added to the experimental chambers prior to sample
158 addition. Since this fluorescent dye is diluted in water, and only a 2 μL volume was added
159 into the 2 mL chamber, no solvent addition was performed in the control group without
160 MgG. After addition of isolated mitochondria into the O2k chambers, residual oxygen
161 consumption R_{ox} was measured in the absence of substrates. Two coupling-control
162 protocols were used to study simultaneously oxygen consumption and ATP production
163 with the following titrations: NADH-pathway with 5 mM pyruvate and 2 mM malate, or
164 Succinate-pathway with 0.5 μM rotenone and 10 mM succinate. First, LEAK respiration
165 was measured in the absence of ADP. Secondly, OXPHOS capacity was measured after
166 addition of 2 mM ADP. Oligomycin (7.5–10.0 nM) or carboxyatractyloside (0.3 – 0.4 mM)
167 were added to induce again a LEAK state. This was followed by stepwise titration of the
168 uncouplers CCCP (0.5 μM steps) or SF 6847 (25–50 nM steps) up to the optimum
169 concentration, when the maximum O_2 flux was achieved as a measure of ET capacity.
170 Finally, residual oxygen consumption was measured after the addition of the CIII inhibitor
171 antimycin A (2.5 μM).

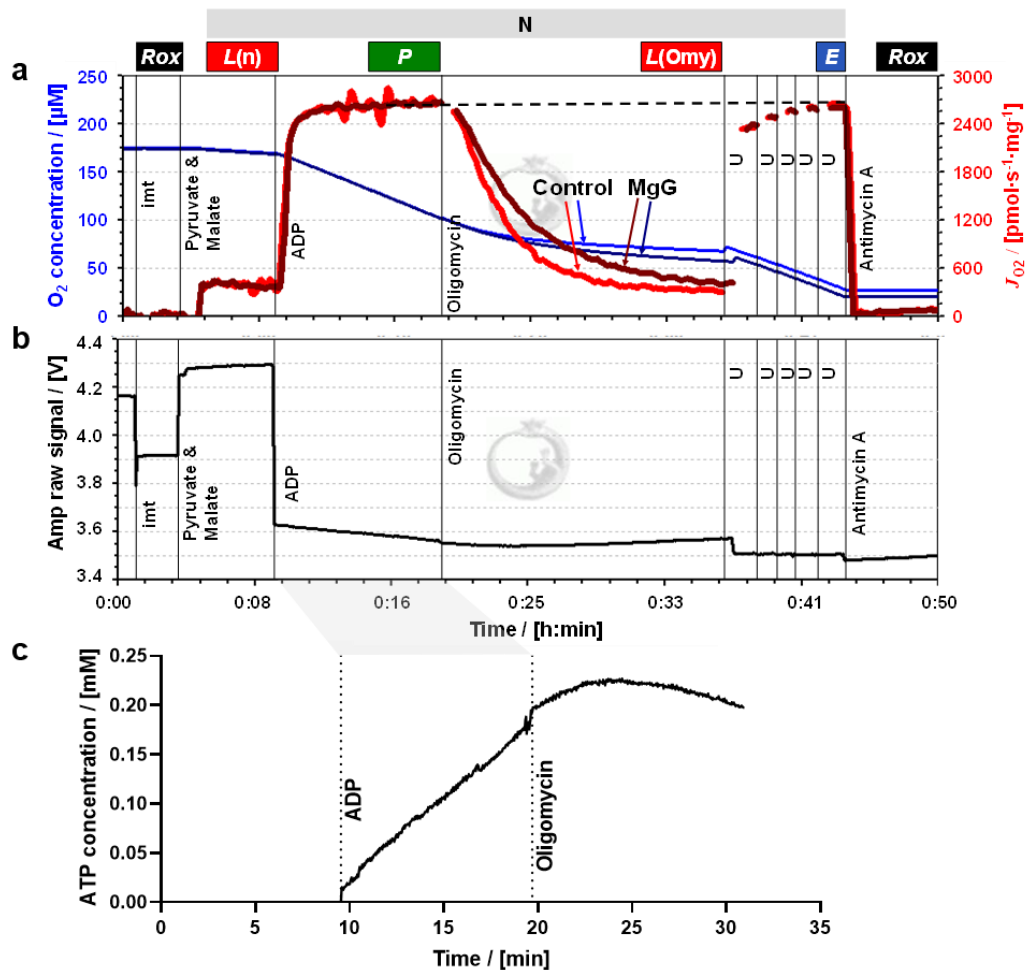
172 2.7. *Data analysis*

173 The assays were repeated 3 times with independent mitochondrial preparations,
174 with or without MgG, for each condition tested. Data analysis for O_2 consumption,
175 calculations of K_d values and ATP production following Chinopoulos et al 2014, were
176 performed using the templates provided with the software DatLab 7.4.

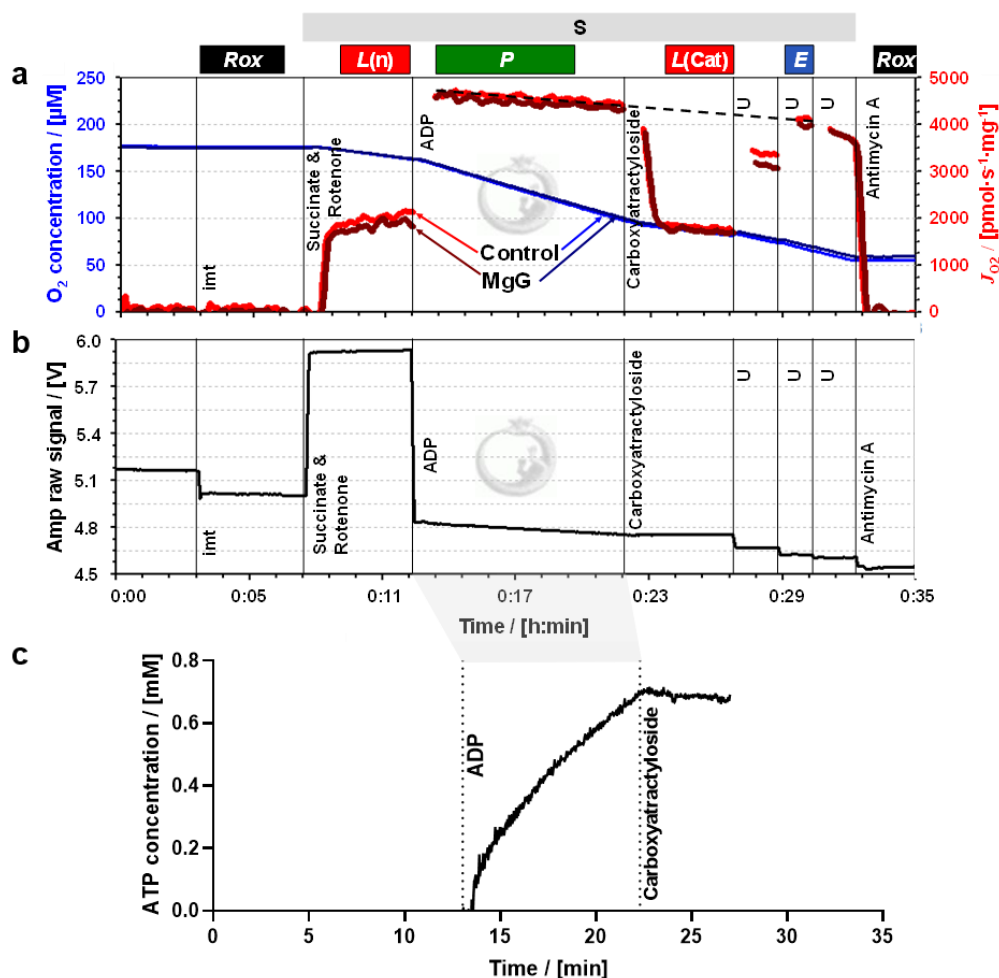
177 3. Results and discussion

178 **Figures 2a and 3a** show superimposed traces of O_2 concentration and O_2 flux per
179 mass. Coupling control of mitochondrial respiration was measured in two different
180 electron-transfer-pathway control states. In the N-protocol, the NADH-linked pathway
181 through Complex I (CI) was evaluated in the presence of pyruvate and malate which
182 stimulate dehydrogenases of the TCA cycle, leading to reduction of NAD^+ to NADH. NADH
183 is the substrate of CI, with further electron flow into the Q-junction, CIII and CIV (**Figure**
184 **2**). In the S-protocol, CI was inhibited by rotenone to prevent reverse electron transfer
185 and accumulation of oxaloacetate, which is an inhibitor of succinate dehydrogenase
186 (Makrecka-Kuka et al 2015; Gnaiger 2020), and respiration was measured supported by
187 succinate as the substrate of CII (**Figure 3**).

188 In both protocols, LEAK respiration was measured (1) $L(n)$, in the absence of
 189 adenylates and (2) $L(Omy)$ or $L(Cat)$, in the presence of phosphorylation system
 190 inhibitors. Respiration in these two LEAK states was similar, but slightly lower in $L(Omy)$
 191 with the N-protocol (Figure 2a, Table 1). $L(n)$ stabilized quickly, whereas for $L(Omy)$ it
 192 took a long time to fully inhibit respiration by the low concentration of 7.5–10.0 nM
 193 oligomycin. In the S-protocol with sequential addition of rotenone followed by succinate,
 194 $L(n)$ increased for a few minutes until stabilization (Figure 3a). Inhibition by
 195 carboxyatractyloside (0.3–0.4 μM) was immediate, and $L(Cat)$ tended to be slightly lower
 196 than $L(n)$ (Table 1).
 197



198 **Figure 2. Simultaneous measurement of respiration and ATP production by high-**
 199 **resolution Fluorespirometry in mitochondria isolated from mouse heart.**
 200 Representative traces for coupling control protocol SUIT-006 with NADH-linked
 201 substrates (N-protocol), following additions (respiratory states): isolated mitochondria
 202 imt (ROX), pyruvate & malate (LEAK), ADP (OXPHOS), oligomycin (LEAK), uncoupler U
 203 (ET), and antimycin A (ROX). Experiment 2019-02-07 P5 04: **(a)** O₂ concentration (dark
 204 and lighter blue traces) and O₂ flux per mass (dark and lighter red), 1.1 μM MgG versus
 205 control; **(b)** MgG fluorescence signal; **(c)** ATP concentration calculated from MgG signal
 206 calibrated as Mg^{2+} concentration.
 207



208
 209 **Figure 3. Simultaneous measurement of respiration and ATP production by high-**
 210 **resolution Fluorespirometry in mitochondria isolated from mouse heart.**
 211 Representative traces for coupling control protocol SUIT-006 with succinate as substrate
 212 (S-protocol), following additions (respiratory states): isolated mitochondria imt (ROX),
 213 succinate & rotenone (LEAK), ADP (OXPHOS), carboxyatractyloside (LEAK), uncoupler U
 214 (ET), and antimycin A (ROX). Experiment 2019-03-18 P5-03: (a) O_2 concentration (dark
 215 and lighter blue traces) and O_2 flux per mass (dark and lighter red), 1.1 μM MgG versus
 216 control; (b) MgG fluorescence signal; (c) ATP concentration calculated from MgG signal
 217 calibrated as Mg^{2+} concentration.

218
 219 OXPHOS capacity P was measured in the presence of a kinetically saturating
 220 concentration of ADP. The optimum uncoupler concentrations to measure maximum ET
 221 capacity E were 6.0–7.0 μM CCCP in the N-protocol, and 0.150–0.175 μM SF 6847 in the
 222 S-protocol. In the N-protocol, P was stable over time and identical to E . However, in the S-
 223 protocol, P showed a slight decrease over time. Extrapolating this trend of declining O_2
 224 flux to the point where ET capacity was measured explains why E appears to be lower
 225 than P (dashed trendline, Figure 3a). In both protocols, therefore, $E = P$, indicating that
 226 OXPHOS capacity was not limited by the phosphorylation system. This agrees with results

227 for mouse heart mitochondria on coupling control even in the combined NS-pathway
228 (Lemieux et al 2017). Parallel measurements were performed in the presence and
229 absence of 1.1 μ M MgG with the N- and S-protocol. This low concentration of MgG used is
230 sufficiently high for calculating ATP production (Figures 2b and c and Figures 3b and c).

231 The MgG assay to measure ATP production can be used concomitantly with high-
232 resolution respirometry, providing information real-time. Other methods are available to
233 detect ATP production real-time. Spectrophotometric detection of NADPH can be used in
234 conjunction with the coupled enzyme system hexokinase and glucose-6-phosphate
235 dehydrogenase (Horgan, 1978). This assay has been adapted for simultaneous detection
236 of O₂ consumption and NADPH (Lark et al 2016). The luciferin/luciferase assay can be
237 used for continuous measurement of ATP production (Manfredi et al 2002). It is
238 important to note that luciferase consumes O₂, and instruments typically used for
239 luminometry do not allow monitoring of O₂ concentration in parallel.

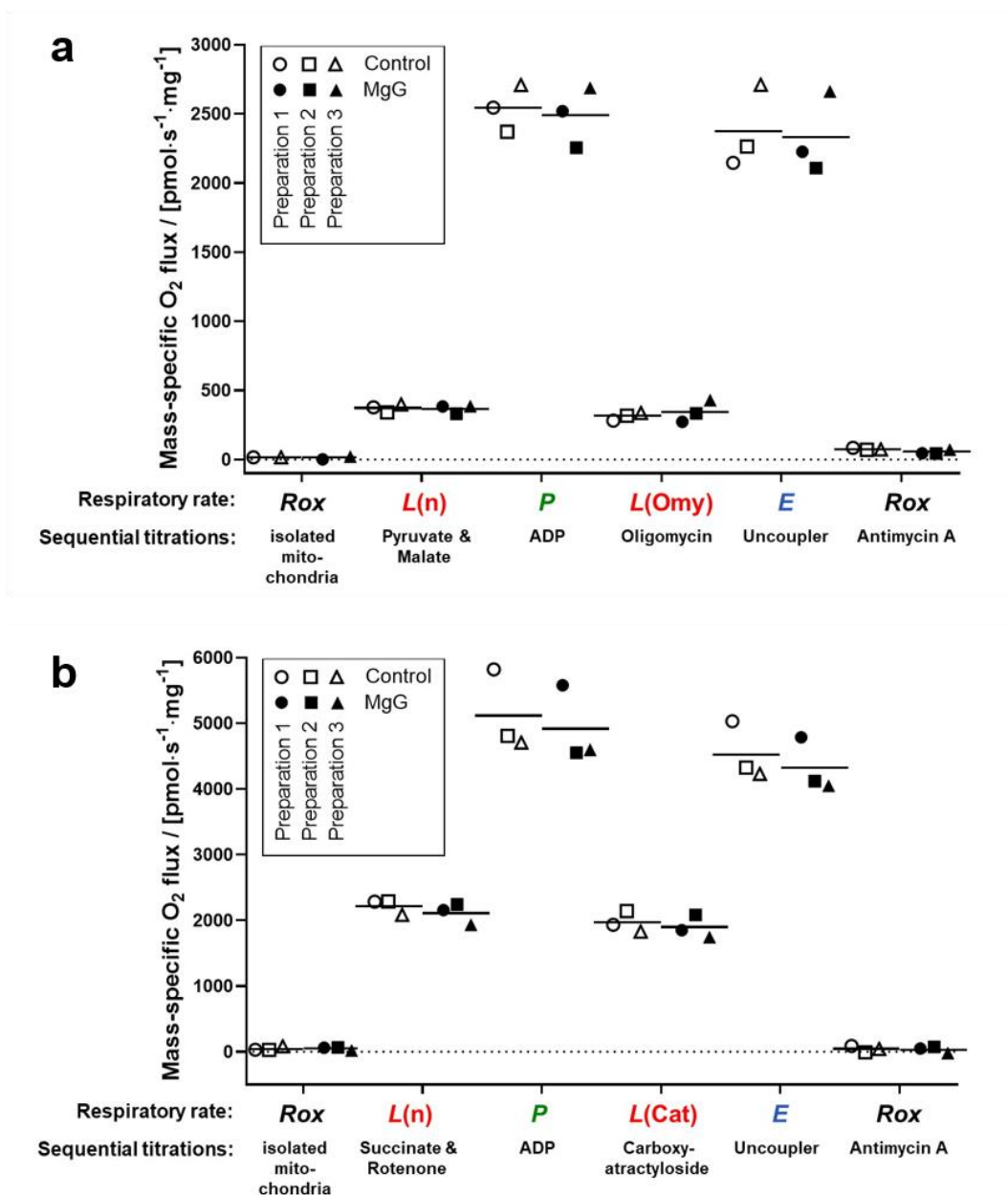
240 Another method for continuous measurement of the P_o/O₂ ratio is the steady-state
241 ADP injection-respirometry (Gnaiger et al 2000b; 2001). The phosphorylation rate is set
242 by continuous injection of ADP as the rate-limiting step while measuring O₂ consumption
243 stimulated to a constant sub-maximal level. Chance and Williams (1955) originally
244 described a polarographic ADP pulse-titration method to determine the P_o/O₂ ratio,
245 titrating a known concentration of ADP, which leads to a peak of O₂ consumption
246 stimulated by the complete phosphorylation of ADP to ATP. The ADP pulse-titration
247 method has been extended and critically discussed by Gnaiger (2001).

248 End-point assays are available to detect ATP levels, providing discontinuous
249 measurement of ATP production. These include chromatography (high performance
250 liquid chromatography, HPLC; thin layer chromatography, TLC); nuclear magnetic
251 resonance detection of 2-deoxyglucose and its phosphorylated form, and radioactivity
252 measurements using ³²P (Menegollo et al 2019; Morciano et al 2017; Fink et al 2017;
253 Sausen et al 2019).

254 The fluorometric MgG assay applied simultaneously with O₂ consumption by HRR
255 has been used extensively (Iftikar, Hickey 2013; Goo et al 2013; Chinopoulos et al 2014;
256 Pham et al 2014; Power et al 2014; Salin et al 2016; Napa et al 2017; Masson et al 2017;
257 Salin et al 2018; Devaux et al 2019; Salin et al 2019). Understanding whether MgG may
258 affect respiration is crucial for such studies, particularly for P_o/O₂ ratios obtained in
259 different electron-transfer-pathway states.

260 It is well established that different dyes commonly applied to measure
261 mitochondrial membrane potential inhibit OXPHOS capacity, *e.g.*, safranin, rhodamine
262 123 and its derivatives TMRM and TMRE (Krumshnabel et al 2014; Scaduto, Grotyohann
263 1999). Surprisingly, Amplex UltraRed used to detect H₂O₂ flux impairs respiration despite
264 not accumulating in the mitochondria (Makrecka-Kuka et al 2015). Therefore, we studied
265 the effect of MgG on respiration. MgG at 1.1 μ M did not affect NADH-linked nor succinate-
266 linked respiration in any coupling control state (LEAK, OXPHOS and ET) measured in
267 mitochondria isolated from mouse hearts (Figure 4). In addition, residual oxygen
268 consumption was not affected by MgG.

269



270
 271 **Figure 4. O₂ consumption in the absence and presence of MgG by mitochondria**
 272 **isolated from mouse heart.** The respiratory rates indicated in the abscissa were
 273 measured by HRR with two coupling control protocols SUIT-006, with the following
 274 respiratory states: ROX, LEAK (in the absence of adenylates), OXPHOS, LEAK (in
 275 the presence of inhibitors), ET, and ROX. Sequential titrations are described for **(a)**
 276 N-protocol (experiments 2019-02-05 P3-04, 2019-02-06 P3-03 and 2019-02-07 P5-04) and
 277 **(b)** S-protocol (experiments 2019-03-13 P6-03, 2019-03-14 P3-03 and 2019-03-18 P5-
 278 03). For both graphs the three symbol shapes show independent mitochondrial
 279 preparations, whereas open and closed symbols compare results in controls and in
 280 the presence of MgG from the same preparation; bars represent the average.
 281

282 **Table 1. Coupling control efficiency $(P-L)/P$ and P_{\gg}/O_2 ratio in absence or presence**
283 **of MgG.** Average \pm SD, $N=3$. OXPHOS capacity P and LEAK respiration L corrected for
284 residual oxygen consumption Rox . $L(n)/L(inh)$ ratios: L in the absence of adenylates (n)
285 over L with an inhibitor (inh) of the phosphorylation system, oligomycin Omy or
286 carboxyatractyloside Cat for the N- or S-pathway, respectively. $L(inh)$ is used in $(P-L)/P$.

Protocol	$(P-L)/P$	$L(n)/L(inh)$	P_{\gg}/O_2	P_{\gg}/O
N-pathway - MgG	0.90 ± 0.01	1.13 ± 0.05	-	-
N-pathway + MgG	0.88 ± 0.02	1.12 ± 0.04	2.33 ± 1.07	1.16 ± 0.53
S-pathway - MgG	0.62 ± 0.05	1.27 ± 0.16	-	-
S-pathway + MgG	0.61 ± 0.05	1.12 ± 0.26	2.78 ± 0.74	1.39 ± 0.37

287
288 The NADH-pathway has three coupling sites, CI, CIII and CIV, whereas the succinate-
289 pathway has only the latter two, resulting in a lower P_{\gg}/O_2 ratio. When dividing ATP flux,
290 calculated from the increase in ATP concentration per time, by the simultaneously
291 measured O₂ flux, then P_{\gg}/O_2 flux ratios ($J_{P_{\gg}}/J_{O_2}$) are obtained. The P_{\gg}/O_2 is twice the
292 classical P_{\gg}/O (Table 1). P_{\gg}/O_2 obtained for S-pathway was close to the theoretically
293 expected value (Gnaiger et al 2020). The result obtained for N-pathway was lower than
294 expected. A limitation of the present study is the low number of replicates ($N = 3$), with a
295 high variability of P_{\gg}/O_2 ratios. Further experiments are in preparation.

296 Coupling control efficiencies are closely related to P_{\gg}/O_2 ratios. The coupling
297 control efficiency is defined as $(E-L)/E$, ranging from 0, at zero coupling, to 1 in a fully
298 coupled system. In the present case of $P = E$, the coupling control efficiency is expressed
299 as the $P-L$ control efficiency, $(P-L)/P$ (Gnaiger 2020). As expected, a higher $P-L$ control
300 efficiency of 0.89 ± 0.02 was found for the N-pathway than 0.62 ± 0.05 for the S-pathway
301 (pooled data with and without MgG, average \pm standard deviation, $N = 6$; Table 1). These
302 correspond to a RCR = P/L of 9.6 ± 1.8 for the N-pathway and 2.6 ± 0.3 for the S-pathway.

303 In summary, MgG did not affect respiration in any of the coupling control states.
304 These results demonstrate that measurement of O₂ consumption is reliable concomitant
305 with the MgG assay in SUIT protocols with different pathway states and coupling states.
306

307 Acknowledgements

308 We thank Marco Di Marcello and Manuela Passrigger for expert technical support on media and
309 chemicals preparation, equipment maintenance and mitochondria isolation. This work was
310 partially funded by the European Union's Horizon 2020 research and innovation programme
311 under grant agreement No. 859770, NextGen-O2k project. Contribution to COST Action CA15203
312 MitoEAGLE.

313 Author contributions

314 LHDC, CD and EG designed the work; LHDC collected and analyzed data and drafted the article;
315 CD and EG critically revised the article, all authors approved the final version of the manuscript.

316 Conflicts of interest

317 EG is founder and CEO of Oroboros Instruments, Innsbruck, Austria.

318 Data availability

319 Original files are available Open Access at Zenodo repository: [10.5281/zenodo.4032674](https://doi.org/10.5281/zenodo.4032674).

320 Abbreviations

321 Amp amperometric; ANT adenosine nucleotide translocase; BSA bovine serum albumin; CI to CIV
 322 Complex I to IV; CCCP carbonyl cyanide m-chlorophenyl hydrazone; $\Delta\Psi_p+$ mt-membrane
 323 potential; EGTA ethylene glycol tetraacetic acid; *E* ET capacity; ETS electron transfer system; F_0F_1
 324 ATP synthase; Hepes *N*-(2-hydroxyethyl)piperazine-*N'*-(2-ethanesulfonic acid); HRR high-
 325 resolution respirometry; imt isolated mitochondria; J_{O_2} O_2 flux; K_d dissociation constant; *L* LEAK
 326 respiration; LED light-emitting diode; MES 2-(*N*-morpholino)ethanesulfonic acid hydrate; MgG
 327 Magnesium Green; *P* OXPHOS capacity; P_{\gg}/O ADP phosphorylated per atom oxygen consumed;
 328 P_{\gg}/O_2 ADP phosphorylated per molecular oxygen consumed; P_i inorganic phosphate; RCR
 329 respiratory acceptor control ratio; *Rox* residual oxygen consumption; SUIT substrate-uncoupler -
 330 inhibitor-titration; TCA tricarboxylic acid; TMRM tetramethylrhodamine methyl ester; TMRE
 331 tetramethylrhodamine ethyl ester; TPP^+ tetraphenylphosphonium; Tris 2-amino-2-
 332 (hydroxymethyl)-1,3-propanediol; U uncoupler.

333 References

- 334 Budinger GRS, Duranteau J, Chandel NS, Schumacker PT (1998) Hibernation during hypoxia in
 335 cardiomyocytes. Role of mitochondria as the O_2 sensor. *J Biol Chem* 273:3320-6.
 336 Chance B, Williams GR (1955) Respiratory enzymes in oxidative phosphorylation. I. Kinetics of oxygen
 337 utilization. *J Biol Chem* 217:383-93.
 338 Chinopoulos C, Vajda S, Csanady L, Mandi M, Mathe K, Adam-Vizi V (2009) A Novel Kinetic Assay of
 339 Mitochondrial ATP-ADP Exchange Rate Mediated by the ANT. *Biophys J* 96:2490-504.
 340 Chinopoulos C, Kiss G, Kawamata H, Starkov AA (2014) Measurement of ADP-ATP exchange in relation to
 341 mitochondrial transmembrane potential and oxygen consumption. *Methods Enzymol* 542:333-48.
 342 Devaux JBL, Hedges CP, Birch N, Herbert N, Renshaw GMC, Hickey AJR (2019) Acidosis maintains the
 343 function of brain mitochondria in hypoxia-tolerant triplefin fish: a strategy to survive acute hypoxic
 344 exposure? *Front Physiol* 9:1941.
 345 Doerrier C, Garcia-Souza LF, Krumschnabel G, Wohlfarter Y, Mészáros AT, Gnaiger E (2018) High-
 346 Resolution FluoRespirometry and OXPHOS protocols for human cells, permeabilized fibers from small
 347 biopsies of muscle, and isolated mitochondria. *Methods Mol Biol* 1782:31-70.
 348 Fink BD, Bai F, Yu L, Sivitz WI (2017) Regulation of ATP production: dependence on calcium concentration
 349 and respiratory state. *Am J Physiol Cell Physiol* 313:C146-53.
 350 Fontana M, Krumschnabel G (2015) Isolation of mouse heart mitochondria. *Mitochondr Physiol Network*
 351 20.06(01):1-2.
 352 Fontana-Ayoub M, Fasching M, Gnaiger E (2016) Selected media and chemicals for respirometry with
 353 mitochondrial preparations. *Mitochondr Physiol Network* 03.02(18):1-10.
 354 Gnaiger E, Wyss M (1994) Chemical forces in the cell: Calculation for the ATP system. In: *What is Controlling*
 355 *Life?* (Gnaiger E, Gellerich FN, Wyss M, eds) *Modern Trends in BioThermoKinetics* 3. Innsbruck Univ
 356 Press:207-12.
 357 Gnaiger E (2001) Bioenergetics at low oxygen: dependence of respiration and phosphorylation on oxygen
 358 and adenosine diphosphate supply. *Respir Physiol* 128:277-97.
 359 Gnaiger E (2020) Mitochondrial pathways and respiratory control. An introduction to OXPHOS analysis. 5th
 360 ed. *Bioenerg Commun* 2020.2: 112 pp. doi:10.26124/bec:2020-0002.
 361 Gnaiger E et al – MitoEAGLE Task Group (2020) Mitochondrial physiology. *Bioenerg Commun* 2020.1.
 362 doi:10.26124/bec:2020-0001.v1.
 363 Gnaiger E, Kuznetsov AV, Schneeberger S, Seiler R, Brandacher G, Steurer W, Margreiter R (2000a)
 364 Mitochondria in the cold. In: *Life in the Cold* (Heldmaier G, Klingenspor M, eds) Springer, Heidelberg,
 365 Berlin, New York:431-42.
 366 Gnaiger E, Méndez G, Hand SC (2000b) High phosphorylation efficiency and depression of uncoupled
 367 respiration in mitochondria under hypoxia. *Proc Natl Acad Sci U S A* 97:11080-5.
 368 Goo S, Pham T, Han JC, Nielsen P, Taberner A, Hickey A, Loiselle D (2013) Multiscale measurement of cardiac
 369 energetics. *Clin Exp Pharmacol Physiol* 40:671-81.

- 370 Horgan DJ (1978) A spectrophotometric assay of ATP synthesized by sarcoplasmic reticulum. *Aust J Biol Sci*
371 31:21-4.
- 372 Iftikar FI, Hickey AJ (2013) Do mitochondria limit hot fish hearts? Understanding the role of mitochondrial
373 function with heat stress in *Notolabrus celidotus*. *PLoS One* 8:e64120.
- 374 Krumschnabel G, Eigentler A, Fasching M, Gnaiger E (2014) Use of safranin for the assessment of
375 mitochondrial membrane potential by high-resolution respirometry and fluorometry. *Methods Enzymol*
376 542:163-81.
- 377 Lark DS, Torres MJ, Lin CT, Ryan TE, Anderson EJ, Neuffer PD (2016) Direct real-time quantification of
378 mitochondrial oxidative phosphorylation efficiency in permeabilized skeletal muscle myofibers. *Am J*
379 *Physiol Cell Physiol* 311:C239-45.
- 380 Lemieux H, Blier PU, Gnaiger E (2017) Remodeling pathway control of mitochondrial respiratory capacity
381 by temperature in mouse heart: electron flow through the Q-junction in permeabilized fibers. *Sci Rep*
382 7:2840, DOI:10.1038/s41598-017-02789-8.
- 383 Leysens A, Nowicky AV, Patterson L, Crompton M, Duchon MR (1996) The relationship between
384 mitochondrial state, ATP hydrolysis, [Mg²⁺]_i and [Ca²⁺]_i studied in isolated rat cardiomyocytes. *J Physiol*
385 496:111-28.
- 386 Lowry OH, Rosebrough NJ, Farr AL, Randall RJ (1951) Protein measurement with the Folin phenol reagent.
387 *J Biol Chem* 193:265-275.
- 388 Makrecka-Kuka M, Krumschnabel G, Gnaiger E (2015) High-resolution respirometry for simultaneous
389 measurement of oxygen and hydrogen peroxide fluxes in permeabilized cells, tissue homogenate and
390 isolated mitochondria. *Biomolecules* 5:1319-38.
- 391 Manfredi G, Yang L, Gajewski CD, Mattiazzi M (2002) Measurements of ATP in mammalian cells. *Methods*
392 26:317-26.
- 393 Masson SWC, Hedges CP, Devaux JBL, James CS, Hickey AJR (2017) Mitochondrial glycerol 3-phosphate
394 facilitates bumblebee pre-flight thermogenesis. *Sci Rep* 7:13107.
- 395 Menegollo M, Tessari I, Bubacco L, Szabadkai G (2019) Determination of ATP, ADP, and AMP Levels by
396 Reversed-Phase High-Performance Liquid Chromatography in Cultured Cells. *Methods Mol Biol*
397 1925:223-32.
- 398 Morciano G, Sarti AC, Marchi S, Missiroli S, Falzoni S, Raffaghello L, Pistoia V, Giorgi C, Di Virgilio F, Pinton P
399 (2017) Use of luciferase probes to measure ATP in living cells and animals. *Nat Protoc* 12:1542-62.
- 400 Napa K, Baeder AC, Witt JE, Rayburn ST, Miller MG, Dallon BW, Gibbs JL, Wilcox SH, Winden DR, Smith JH,
401 Reynolds PR, Bikman BT (2017) LPS from *P. gingivalis* negatively alters gingival cell mitochondrial
402 bioenergetics. *Int J Dent* 2017:2697210.
- 403 Pham T, Loisel D, Power A, Hickey AJ (2014) Mitochondrial inefficiencies and anoxic ATP hydrolysis
404 capacities in diabetic rat heart. *Am J Physiol* 307:C499-507.
- 405 Power A, Pearson N, Pham T, Cheung C, Phillips A, Hickey A (2014) Uncoupling of oxidative phosphorylation
406 and ATP synthase reversal within the hyperthermic heart. *Physiol Rep* pii:e12138.
- 407 Salin K, Villasevil EM, Auer SK, Anderson GJ, Selman C, Metcalfe NB, Chinopoulos C (2016) Simultaneous
408 measurement of mitochondrial respiration and ATP production in tissue homogenates and calculation
409 of effective P/O ratios. *Physiol Rep* 10.14814/phy2.13007.
- 410 Salin K, Villasevil EM, Anderson GJ, Selman C, Chinopoulos C, Metcalfe NB (2018) The RCR and ATP/O
411 indices can give contradictory messages about mitochondrial efficiency. *Integr Comp Biol* 58:486-94.
- 412 Salin K, Villasevil EM, Anderson GJ, Lamarre SG, Melanson CA, McCarthy I, Selman C, Metcalfe NB (2019)
413 Differences in mitochondrial efficiency explain individual variation in growth performance. *Proc Biol Sci*
414 286:20191466.
- 415 Sausen CW, Rogers CM, Bochman ML (2019) Thin-Layer Chromatography and Real-Time Coupled Assays
416 to Measure ATP Hydrolysis. *Methods Mol Biol* 1999:245-253.
- 417 Scaduto RC Jr, Grotyohann LW (1999) Measurement of mitochondrial membrane potential using
418 fluorescent rhodamine derivatives. *Biophys J* 76:469-77.

420 **Copyright:** © 2021 The authors. This is an Open Access preprint (not peer-reviewed) distributed
421 under the terms of the Creative Commons Attribution License, which permits unrestricted use,
422 distribution, and reproduction in any medium, provided the original authors and source are
423 credited. © remains with the authors, who have granted MitoFit Preprints an Open Access
424 publication license in perpetuity.

